Anisotropy in Magnetism

Klaus Baberschke

Institut für Experimentalphysik, Freie Universität Berlin, Arnimallee 14,
D-14195 Berlin, Germany

Abstract. The enormous research on magnetic properties of ultrathin films and nanostructures produces also new activities in the fundamental understanding of the magnetic anisotropy energy (MAE) and the anisotropy of the orbital magnetic moment/atom. The pseudomorphic growth of Fe, Co, Ni on metallic and non-metallic substrates can change the nearest neighbor distance by ≈ 0.05 Å. This small change in structure and symmetry increases the MAE by several orders of magnitude and lifts the quenching of the orbital moment. Increases of $20 - 30\%$ of the orbital moment μ_{L} are observed. This experimental finding is confirmed by full relativistic ab initio calculations. Various experiments deliver the full temperature dependence of all MAE contributions. The temperature dependence remains a challenge for the theory in itinerant magnetism.

1 Introduction

The anisotropy in magnetic phenomena is well established in theoretical and experimental investigations. We refer to standard textbooks, e.g. [1–4]. Although this is common knowledge and standard part of teaching in solid state physics, in recent years a revival happened with an enormous number of new results and publications, in particular for itinerant magnets. In our opinion this has at least three independent reasons:

- There is an obvious interest on ultrathin ferromagnetic films and nanostructures for technological applications (we refer to recent reviews [5,6]).
- In 1985-87 the magnetic circular dichroism was introduced in the x-ray regime (XMCD = **X**-ray **M**agnetic **C**ircular **D**ichroism). This new experimental technique became very popular when circular polarized synchrotron radiation was available [7,8]. Theoretical efforts followed immediately [9]; using a localized picture to calculate the transition probability at the $\mathrm{L}_{3,2}$-edges of 3d ferromagnets, the so-called 'sum rules' were developed [9–11].
- Advances in *ab initio* theories and computational capacities allow today full relativistic calculation of the total energy and its magnetic anisotropic contributions [12–14]. In section 2 we will show that the anisotropic magnetic energy is in the order of $\approx \mu$eV/atom out of some eV/atom of the total energy. In other words, total energy calculations for particular systems are that precise and reliable that $\approx 10^{-6}$ contributions can be calculated (analogy in 1960's can be seen for the core polarization in the hyperfine fields).

We prefer to see these three reasons (and more) as an accidental 'coincidence'. It is not only the demand for new technologies in magnetic storage media, but also the progress in the fundamental understanding which reactivate the discussion of magnetic anisotropies. I.e. in the history of magnetism [15] the MAE was always treated in a thermodynamical phenomenological way by expanding the free energy [16]. In nowadays magnetism is interpreted from an atomistic, microscopic point of view: New artificial structures can be grown with different symmetries and lattice constants (changes by few 1/100 Å only). These real structures serve as input for *ab initio* theories (see the chapters by R. Q. Wu and O. Eriksson in this book) and it appears that these small changes in the nearest neighbor distance (≈ 0.05 Å) change the magnetic anisotropy energy by 2-3 orders of magnitude! This will be a main aspect of the present contribution.

Table 1. Characteristic energies of metallic ferromagnets (MAE values are given at room temperature) [17]

binding energy	$1 - 10$ eV/atom
exchange energy	$10 - 10^3$ meV/atom
cubic MAE (Ni)	0.2 μeV/atom
uniaxial MAE (Co)	70 μeV/atom

Unfortunately the history of magnetism and magnetic anisotropy went different routes and were uncoupled from other areas of solid state magnetism, that is to say, magnetoelastic theory had sometimes very little contact with crystal field theory (e.g. [18]). As a consequence, the classification of magnetic anisotropy contribution went a different route than Legendre polynom expansion in crystal field theory. Moreover, as a consequence various units are used in the historical part of magnetoelasticity, namely erg/cm^3 and erg/cm^2, that is to say energy per volume and area, respectively. Other parts of solid state physics and in particular the theory prefers eV/atom, that is to say energy per particle (see Tab.1). This newer notation started to be used in surface and thin film magnetism and we strongly advocate in favor of it, since it facilitates the communication with theory and gives an easier insight. For example, in thin film magnetism Fe, Co and Ni ions contribute equally strong to the anisotropy energy, be it a surface atom or an atom in the inner part of a nanostructure, namely $10-100$μeV/atom. In the older version it would read $1.5 - 15 \cdot 10^6$ erg/cm^3 and $0.03 - 0.3 \cdot$ erg/cm^2 which is not so easy to be compared.
In the following we distiguish only two effects of anisotropy in magnetism:

- In Sec.2 we discuss the magnetic anisotropy energy (MAE), which is the energy to rotate the magnetization of a single magnetic domain from its easy axis into the hard axis. At first glance this energy is largest at $T = 0$ and reduces to 0, if T approaches the ordering temperature T_C [16]. On a

closer look we note that details of the temperature dependence depend on the origin of the anisotropy, namely a single particle or pair interaction [1]. Gd metal for example has a finite anisotropy above T_C [3,17].

- In Sec.3 we discuss the anisotropic magnetic moment/atom. This is in first order a *temperature independent* observable and originates from the anisotropic orbital magnetic moment which is in films and nanostructures not fully quenched.

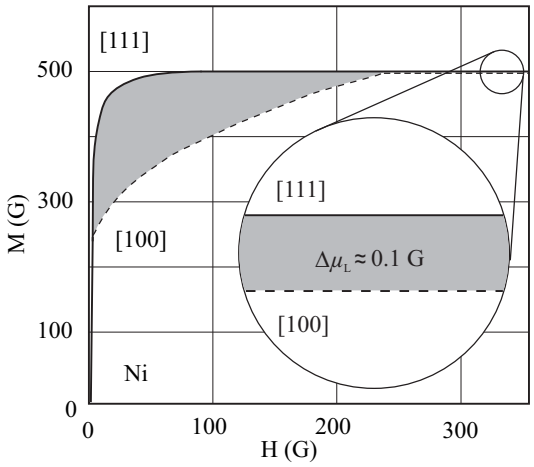

Fig. 1. Room temperature magnetization curve for Ni along the easy ([111]) and hard ([100]) direction [17]

Both effects are schematically shown in Fig.1: The MAE corresponds to the gray triangle and amounts at 300 K to $\approx$ 0.2 μeV/atom for fcc Ni (Tab.1). The anisotropy in the magnetic moments $\Delta\mu_L/\mu \approx 10^{-4}$ for bulk cubic Ni. In the following we will see that both may increase by orders of magnitude for nanostructures. The latter effect survives far in the paramagnetic regime. It is well known [17] that the magnetic moments of Fe, Co, Ni are larger along the easy axis (see inset of Fig.1) than in other directions.

2 Magnetic Anisotropy Energy (MAE)

In common phenomenology of MAE several origins can be listed: magneto-crystalline, magneto-elastic, etc.. In view of its physical origin we prefer to distinguish only two types:

- The intrinsic anisotropy K. It originates from the non spherical charge distribution, be it in a localized or itinerant picture. It is the only mechanism for

anisotropic energy in an infinite sized crystal (here we ignore the small dipolar contributions for non cubic symmetry). As discussed in Sec.1 this can be treated in *ab initio* theories in full-relativistic and full-potential treatments.
- The only other mechanism is the dipole-dipole interaction which may become dominant in finite sized samples. It depends entirely on the sample shape.

In the following we discuss exclusively 'single-domain physics' for two reasons: (i) There exist excellent literature for multi-domain magnetism [19]. (ii) The thermodynamic ground state for many nanostructures investigated in recent literature is a single domain state. Note that for example ultrathin Co/Cu(001) films of few atomic layers thickness is a single domain system in its thermodynamic ground state with easy axis in plane. This is not in contradiction to PEEM microscopy. There, the as grown film shows a multi-domain state which is not the thermodynamic ground state of the system. Depending on stiffness constant and other parameters all structures with dimensions smaller than a few nm are single-domain in the ground state [1]. In the following we use the letter 'K' exclusively for this intrinsic anisotropy (orbital moment induced), it is the focal point of the experiments presented here. The experimentally measured total value of the MAE includes also the dipolar contribution, which can be calculated (Sec.2.2) and is subtracted from the raw experimental data before discussing the intrinsic MAE 'K'.

2.1 Intrinsic Anisotropy K

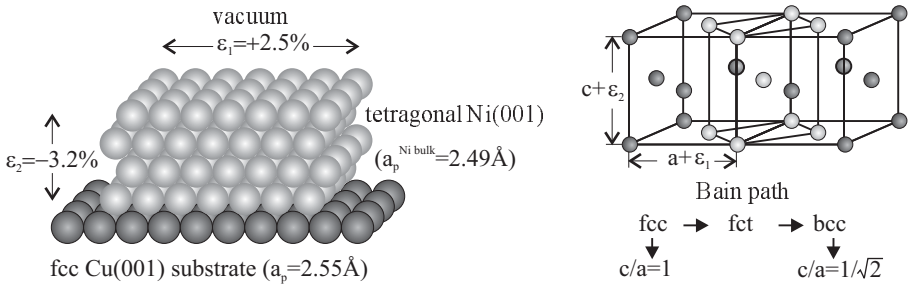

Fig. 2. Schematic drawing of pseudomorphic growth of Ni on a Cu(001) substrate. On the right hand side an fcc lattice is shown for $c/a = 1$. If the c/a-ratio reduces down to $c/a = 1/\sqrt{2}$, the lighter spheres indicate the new bcc lattice cell. [20]

In Fig.2 an ultrathin film grown in register on a substrate crystal is shown schematically, e.g. Ni/Cu(001). The nearest neighbor distance in bulk Cu is $a_{\mathrm{Cu}} = 2.55$ Å and in Ni $a_{\mathrm{Ni}} = 2.49$ Å. The pseudomorphic growth of Ni on Cu(001) results in an in-plane tensile strain of $\varepsilon_1 = 2.5$ %. Keeping the total energy at a minimum or $\delta \mathrm{V} = 0$ results in a contraction along the c-axis of

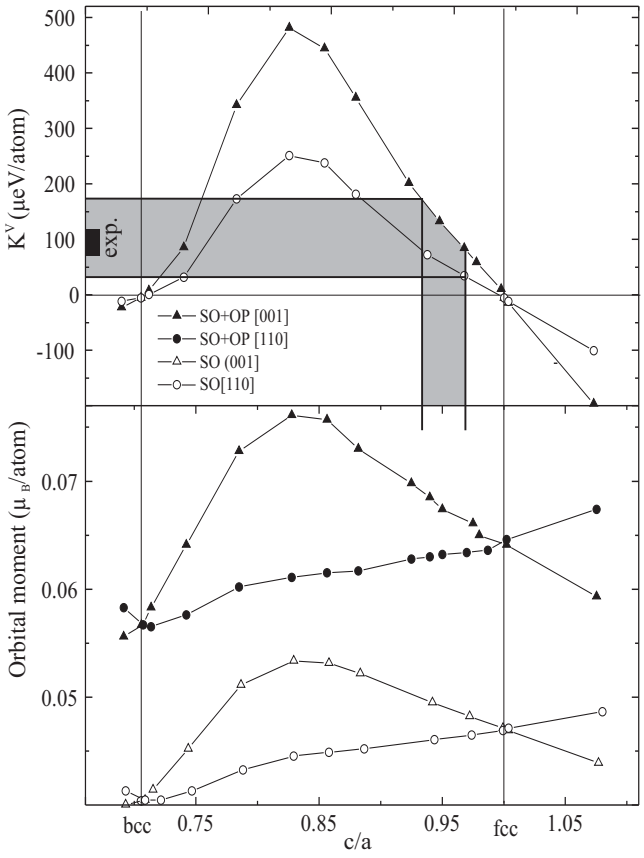

Fig. 3. An all electron and full relativistic calculation of the intrinsic anisotropy K and anisotropy of the orbital moment for an infinitely sized Ni single crystal as function of uniaxial deformation of the c/a-ratio [21]. All symbols are calculated values for two crystallographic orientations. Open symbols correspond to spin-orbit-coupling-only, full symbols to SO+orbital polarization(OP). The grey area on the x-axis indicates the uncertainty of the c/a-ratio from LEED measurements [22]. This uncertainty can be projected on the y-axis, depending on SO-only or SO+OP calculations. It results in an anisotropy energy of the order of 100 μeV/atom, which agrees nicely with the experiments [23].

$\varepsilon_2 = -3.2$ %. In other words, the cubic symmetry of Ni reduces to a tetragonal symmetry, face centered tetragonal (fct). In the right panel of Fig.2 this lattice is schematically shown. If one compresses the c-axis down to $c/a = 1/\sqrt{2}$, we end up again in cubic symmetry (light spheres) with a bcc lattice (the so-called Bain path, see the chapter by O. Eriksson in this book). Hjortstam et al. [21] have calculated for such an artificial structure with infinite size the total energy E as well as the magnetic anisotropy energy (see Fig.3).

$$K = \Delta E = E_{[001]} - E_{[110]} \tag{1}$$

At exact cubic fcc and bcc symmetry $K \approx 0$ μeV/atom (see Tab.1). This calculation shows very nicely that K increases dramatically by orders of magnitude, if Ni departs from cubic symmetry. Similar calculations have been performed by Wu et al. for Co/Cu(001) [24]. Fig.3 shows also the difference between spin-orbit(SO)-only calculations and adding orbital polarization (OP) (for details see theoretical contributions by O. Eriksson and R. Q. Wu in this volume). Oversimplifying one might say that SO-only calculation corresponds to Hund's third rule, namely the coupling of the orbital (L) and spin momentum (S). The SO- and SO+OP-calculation in Fig.3 shows that there is a significant difference, a detailed discussion goes beyond this contribution, but the figure shows clearly that the non-spherical charge distribution ($L \neq 0$) contributes significantly to the intrinsic magnetic anisotropy energy. Strictly speaking, the non-vanishing orbital momentum (non-spherical charge distribution) is the only origin of the intrinsic MAE (it includes magneto-elastic, magneto-crystalline and other effects). For Ni/Cu(001) the c/a-ratio was determined to be $c/a \approx 0.95$ [22]. The hatched area in Fig.3 shows nicely that this ends up in a MAE of $K \approx 100$ μeV/atom. In Sec.3 we will discuss the lower panel of Fig.3, showing the anisotropy of μ_{L}. So far we have not included any surface or interface effects. Fig.4 shows schematically the K^{S1}, the surface facing vacuum and the interface regime K^{S2}. Following Néel [25] and Gradmann [26] one can decompose the total intrinsic 'K' of a thin film into a surface and interface effect and into a contribution arising from the inner part, the so-called K^{V}, where 'V' stands for volume.

$$K_{\mathrm{i}} = K_{\mathrm{i}}^{\mathrm{V}} + \frac{2K_{\mathrm{i}}^{\mathrm{S}}}{d} \tag{2}$$

Note that this is an energy density and consequently the first term K^{V} is a constant contribution originating from the inner part of the sample. The second term in Eq.(2) yields an average term for the surface contribution K^{S}, which contributes with $1/d$ to the total K. The subscript i stands for various contributions of K being explained in Sec.2.3.

In the right part of Fig.4 we show for Ni/Cu(001) that the experimentally determined K follows exactly the linear dependence of $K \propto 1/d$. To our experience this is the most sensitive method to determine real pseudomorphic growth. For Ni/Cu(001) we have found that Ni grows pseudomorphically in a fct structure up to $d \approx 15$ ML. For thicker films with $d \geq 20$ ML the system relaxes (producing misfit dislocations) into its original bulk fcc structure, while the MAE decreases again to $K \to 0$. Performing experiments for various thicknesses in the range of $2 - 10$ ML one also changes the Curie temperature of the ferromagnet due to finite size effects. Therefore, it is all important to plot this type of diagram as function of the reduced temperature $t = T/T_{\mathrm{C}}$. Fig.4 shows this for $t = 0.56$ and $t = 0.74$. If, for example, thickness dependent measurements are performed only at ambient temperature, $T \approx 300$ K, the $K(1/d)$-plots are misleading and lead to wrong conclusions, as we have shown recently for Co/Cu(111) [27].

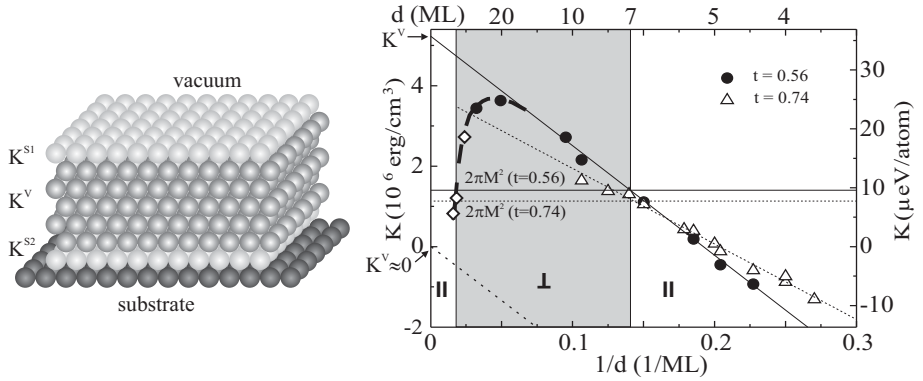

Fig. 4. Left panel: Schematic drawing of a pseudomorphic grown thin film with 3 contributions of anisotropy energy contributions, the surface term K^{S1}, the interface term K^{S2} and the central or volume term K^{V}. Right hand panel: Experimental data for Ni/Cu(001) taken from [28]. If, hypothetically, the Ni film would grow in a pseudomorphic structure up to infinite thickness ($1/d = 0$), K^{V} would reach a value indicated on the y-axis. This is by orders of magnitude larger than for unperturbed bulk fcc Ni as indicated close to the '0' of the y-axis. The 3 regimes indicate parallel, perpendicular and again parallel easy axis of magnetization. For details of the spin reorientation transition see [28,30].

In earlier literature of thin film magnetism it has been said that the Néel (surface) contribution to the MAE is dominant because of symmetry breaking and is the main reason for large MAE in ultrathin films. Such a statement would be only true, if the inner part of a thin film would not contribute to the MAE, which is in obvious contrast to Fig.4. In nowadays the high precision of surface structure analysis techniques proves that most of the grown nanostructures in thin films do not have bulk cubic symmetry, but perturbed lower symmetric artificial structures. The extrapolation of $K(1/d)$ in Fig.4 shows clearly that for $1/d \to 0$ we end up with a $K^{\mathrm{V}} \approx 30$ μeV/atom at a reduced temperature of $t = 0.56$ which is two orders of magnitude larger than for bulk Ni (Fig.1, Tab.1). This simple argumentation has been nicely proven in the theoretical calculation by Uiberacker et al. [29], displayed in Fig.5. They have taken a thin film of 12ML of Ni, facing on the right hand side the vacuum surface and on the left the Cu substrate. The surface layer (layer 15 in Fig.5) gives a huge negative contribution corresponding to the negative slope in Fig.4. They also found a negative contribution at the interface layer (layer 4), but less dramatic than in the vacuum facing surface. In the present context however, it is most important to see that the central part of the film (layers 5 to 14) also contributes very much to the magnetic anisotropy, if the cubic symmetry is broken. For -5.5 % relaxation approximately 10 layers contribute each with $K \approx 100$ μeV/atom. This overcomes definitely the surface and interface contribution which count only for 1 layer.

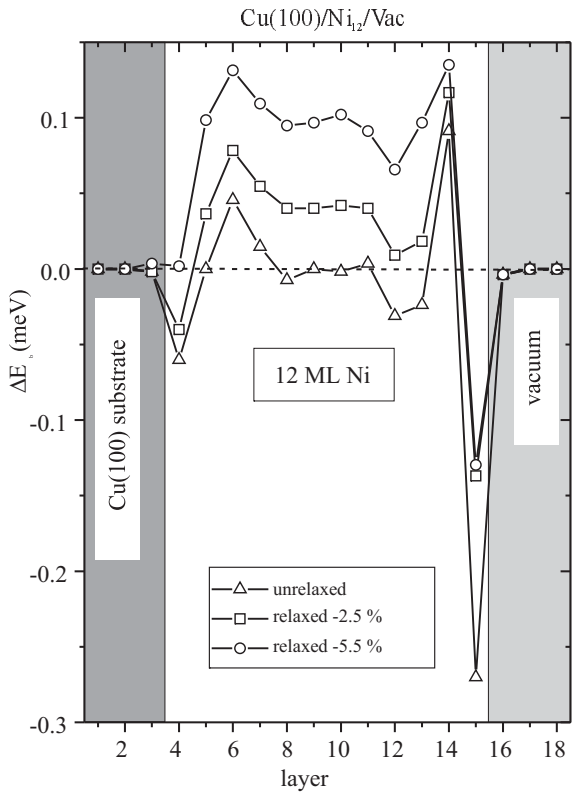

Fig. 5. Magnetic Anisotropy energy calculated for 12 ML Ni/Cu(001) [29]. The energy difference ΔE, defined in Eq.1, was calculated for each layer, starting with 3 layers of Cu substrate, followed by 12 layers of Ni atoms and 3 layers on the vacuum side above Ni. The open triangles denote an unrelaxed, cubic fcc-lattice, squares and circles correspond to a relaxed tetragonal structure.

In summary, for the analysis of MAE in nanostructures and ultrathin films it is all important to consider the real structure and symmetry and not to assume that the inner part of the structures behave like bulk cubic Fe or Ni. High precision structure analysis of these materials serves as an ideal input for theoretical *ab initio* calculations. In previous publications we have discussed thickness and temperature dependent spin reorientation transition [30]; for the present focus it is all important to note that the main reason for the reorientation is the above discussed K^{V} contribution of the fct Ni. Only the tetragonal distortion produces in Fig.4 an intercept of the y-axis at large K-values. Taking the same negative slope (negative K^{S}), but assuming a cubic fcc structure $K(1/d)$ would cross the y-axis at $K \approx 0$ (dotted line in Fig.4), resulting in the fact that the Ni film would never have an easy axis perpendicular to the film plane. So far all theoretical

calculations were done for $T = 0$, but experiments were not. We will come back to this in Sec.2.3.

2.2 Dipolar (shape) Anisotropy

The only other anisotropic interaction between magnetic moments $\boldsymbol{\mu_i}$ and $\boldsymbol{\mu_j}$ with a distance of $\boldsymbol{r_{ij}}$ is the dipole-dipole interaction:

$$H_{\mathrm{dip}} = \sum_{i \neq j} r_{\mathrm{ij}}^{-3} \left[(\boldsymbol{\mu_i} \cdot \boldsymbol{\mu_j}) - \frac{3}{r_{\mathrm{ij}}^2} (\boldsymbol{\mu_i} \cdot \boldsymbol{r_{ij}}) (\boldsymbol{\mu_j} \cdot \boldsymbol{r_{ij}}) \right] \tag{3}$$

The second term in the dipolar interaction shows clearly that the dipole energy depends on the orientation of the magnetic moments $\boldsymbol{\mu_i}$, $\boldsymbol{\mu_j}$ with respect to $\boldsymbol{r_{ij}}$: E_{dip} is lowest, if the magnetization $\boldsymbol{M}$ points parallel to $\boldsymbol{r_{ij}}$ and it costs energy to rotate the two dipole moments perpendicular to the the $\boldsymbol{r_{ij}}$-axis. This simple argument demonstrates clearly that an exchange coupling by $J\boldsymbol{S_i} \cdot \boldsymbol{S_j}$ is per definition isotropic. A scalar product $\boldsymbol{S_i} \cdot \boldsymbol{S_j}$ does not depend on the space coordinates, i.e. the exchange energy depends on the angle between the neighboring spins, but is independent of their orientation relative to their bond direction. Consequently, it costs no energy to rotate two spin moments in space as long as one keeps them parallel or antiparallel to each other. It is worth-while to note that a so-called anisotropic exchange interaction cited in the literature originates from the projection of spin-orbit coupling into spin space. One may project part of the orbital momentum and interaction into spin space. We prefer to keep the orbital magnetism as what it is, originating from non-spherical charge distributions described by the orbital angular momentum, be it as orbital polarization or as spin-orbit coupling. Another quite common way of interpretation for 3d ferromagnetism is to state a quenching of the orbital momentum and replace the magnetic moment $\boldsymbol{\mu}$ by a spin vector $\boldsymbol{S}$ resulting from Eq.(3) with an 'effective anisotropic exchange'.
The summation over all lattice sites i, j in cubic symmetry and infinite-sized samples vanishes. We know that for non-cubic specimen like hcp cobalt or fct Ni small finite dipolar contributions remain, even if the sample is infinite-sized as discussed in the beginning of Sec.2.1 (we ignore this in the following discussion). For finite-sized samples like ultrathin films two approaches are commonly used:

- *The continuum model* assuming a dipole density: This leads to the well-known demagnetizing factor N times the magnetization M^2:

$$E_{\mathrm{dip}} = 2\pi \left(N_{\perp} - N_{||} \right) M^2 \tag{4}$$

- The *discrete lattice sum* over point dipoles: Here a magnetic moment per lattice site is assumed and the summation (Madelung-sum) is taken over the whole specimen.

Today's experiments in metallic ferromagnets and ultrathin films are that precise and demonstrate that non of the two models is good enough. In the continuum

model one cannot assume that $N_{||} = 0$ is and $N_{\perp} = 1$ respectively. A better approximation is $N_{||} \approx \frac{\pi d}{4D}$, where d is the film thickness and D the diameter of the film. $N_{||}$ can directly be measured via susceptibility experiments because the maximum in the susceptibility peak is limited by $1/N_{||}$:

$$\chi_{\text{exp}} = \frac{1}{\frac{1}{\chi_{\text{int}}} + N_{||}} \tag{5}$$

In recent susceptibility measurements of ultrathin Gd films we have measured $\chi_{\text{max}} \approx 10^4$ for films in the order of 1 nm thickness. From that we deduced that the lower limit for the lateral diameter is in the order of $D \approx 0.5$ μm [31]. This was later confirmed in a STM experiment [32]. Summation over discrete dipoles has been performed in bulk and ultrathin films [33,34]. This leads to a small demagnetizing energy [33,34]. In conclusion: The true demagnetizing energy lies between the two limits. What needs to be done in the future is the calculation of a lattice sum using a finite magnetic moment profile (measured by neutron form factor analysis, for example).
Another and more important effect is to consider the proper temperature dependence $M(T)$. In the next section we will discuss the temperature dependence of the intrinsic anisotropy 'K'. A priori it is not clear that the temperature dependence $K(T)$ and $M(T)$ are known or well understood. In earlier literature of thin film magnetism an effective anisotropy was introduced as the sum of two contributions $K_{\text{eff}} = K + 2\pi M^2$. Since $K(T)$ and $M(T)$ may have a completely different temperature dependence $f(T)$, be it an analytical function or not, the sum of the two and an effective K mixes both effects and makes the situation less transparent. A more transparent way of analysis is to separate immediately the temperature dependence of dipolar interaction $M^2(T)$ and the intrinsic anisotropy $K(T)$ and discuss both contributions separately, even if a very precise temperature determination of E_{dip} is still not available.

2.3 Angular and Temperature Dependence of the MAE

Following Eq.(3) the dipolar anisotropy is described in a reasonable approximation by a $\cos^2(\theta)$-law. The intrinsic anisotropy 'K', however, consists out of several contributions with twofold, fourfold, etc. symmetry following a $\cos^2(\theta)$-,$\cos(2\varphi)$-, $\cos^4(\theta)$-, $\cos(4\varphi)$-, ... angular dependence. For the anisotropy of bulk ferromagnets this is well tabulated in the literature [1–3]. We note that there exists no common nomenclature. In [3] one finds an expansion in Legendre polynoms (in analogy to crystal field theory), whereas in [1,2] one finds an expansion in trigonometrical functions. The latter is listed in [17]. Unfortunately no unique systematic has been used in the majority of literature on thin film magnetism, most publications use only an effective uniaxial term. In Eq.(6) we give some frequently used notation for the intrinsic free energy density for systems of tetragonal symmetry:

$$E = E_{\text{eff}} - E_{\text{dip}} = -K_{2\perp} \cdot \cos^2(\theta) - K_{2||} \cdot \cos(2\varphi) \sin^2(\theta) - \\ -\frac{1}{2} K_{4||} \frac{1}{4} [3 + \cos(4\varphi)] \cdot \sin^4(\theta) - \frac{1}{2} K_{4\perp} \cdot \cos^4(\theta) + \ldots \tag{6}$$

We note here that this expansion of the anisotropy energy is used by the majority but it has also some disadvantages: Legendre polynom expansion used in [3] has the advantage that one finds a monotonic decrease as function of temperature and not a crossing of the sign as it is listed e.g. for Fe, Co and Ni in [17]. The higher (fourth) order terms are of principle importance because only a higher than quadratic function in the free energy can lead to energy minima (easy axis of magnetization) at arbitrary angles. That is to say all interpretations of thin film magnetism which restrict themselve to an uniaxial $\cos^2(\theta)$-dependence will find only easy axis being in- or out-of-plane. However there exist examples (prototype Ni/Cu(001)) with a continuous rotation of the easy axis [35–37]. A detailed description of this effect has been given in [38]. In Fig.6 we demonstrate these dependencies for a Fe_4/V_4-multilayer. For this multilayer structure the ferromagnetic resonance was measured angular dependent as function of the polar angle θ_H and the azimuthal angle φ_H.

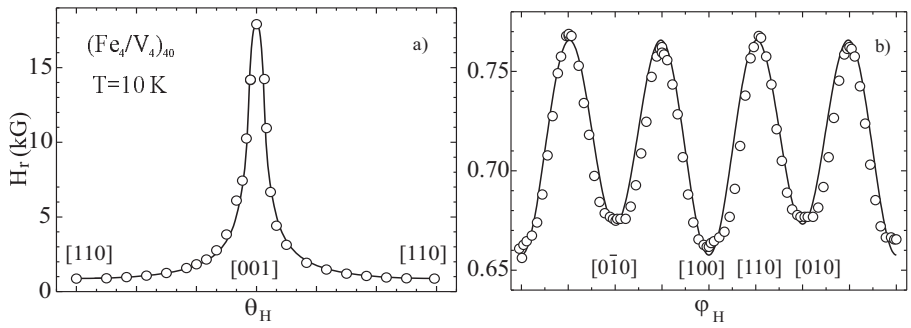

Fig. 6. Polar (θ_H) and azimuthal (φ_H) angular dependence of the FMR resonance field H_r for a Fe_4/V_4-multilayer at 10 K [36].

In Fig.6 we clearly see a 180°-dependence with the resonance field H_r being largest along the film normal [001] (i.e. the hard axis) and H_r being lowest in the film plane [100] (i.e. easy axis). It is all important to measure the full angular dependence as indicated by the open circles and to fit it to the Eq.(6). We note that measuring only the hard axis and easy axis leads to a misinterpretation of pseudo-uniaxial symmetry. The fitted solid line has very large components of fourth order terms (for details see [39]). On the right hand panel we show the azimuthal in-plane angular dependence which is obviously smaller and superimposes a 90°- and 180° angular dependence. The very small 180° angular dependence is produced by steps within the surface plane of the film structure.

In Fig.7 we show the K_2, $K_{4\perp}$ and $K_{4||}$ as function of temperature. First of all we note that K_2 and $K_{4\perp}$ are in the same order of magnitude at low temperature (left hand y-axis) but of opposite sign. $K_{4\perp}$ is negative, whereas K_2 is positive. The in-plane component $K_{4||}$ is about one order of magnitude smaller than the out-of-plane contributions (right hand y-axis). The ferromagnetic resonance is the technique of choice to measure each of these contributions also as function of temperature. The experimental results shown in Fig.7 reveal that each has a different temperature dependence.

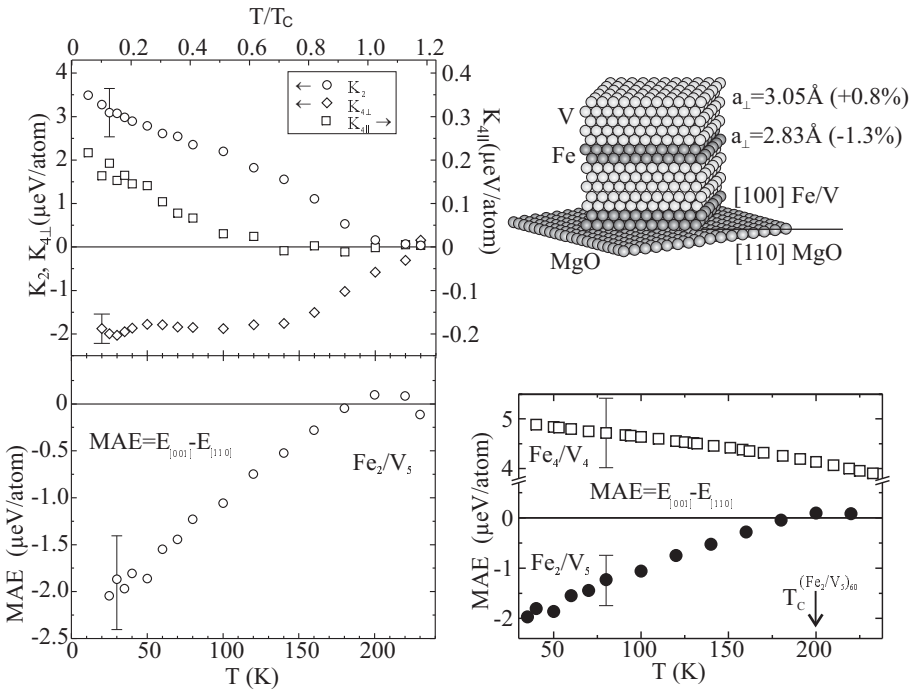

Fig. 7. Schematic drawing of a Fe_2/V_5-multilayer structure grown on an MgO single crystal. Temperature dependence of the various anisotropy components K_i as function of the absolute and reduced temperature for both multilayer structures Fe_2/V_5 and Fe_4/V_4 [39].

In the lower panel we show similar results for a thinner Fe_2/V_5 film. From the lower right hand part of Fig.7 it is obvious that Fe_4/V_4 and Fe_2/V_5 show completely different temperature dependencies. This again is an unambiguous demonstration that not only the interface term at the Fe/V-interface contributes to the anisotropy but also the layer 2 and 3 in the film of 4 ML Fe.
A similar type of analysis has been performed for our prototype system Ni/Cu(001). For various samples ranging between 7 and 8 ML a full set of angu-

lar dependent FMR measurements over a large range of reduced temperatures $t = 0.2 - 0.9$ were performed (Fig.8). Again K_2 and $K_{4\perp}$ have different signs. For $T \to 0$ K_2 is only about 3 times larger than $K_{4\perp}$. The fourfold in-plane anisotropy $K_{4||}$ is smaller by about one order of magnitude.

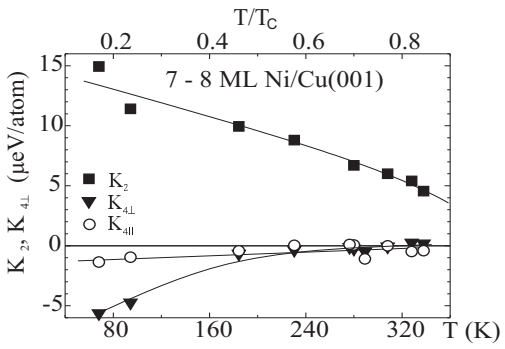

Fig. 8. Temperature dependence of K_2, $K_{4\perp}$ and $K_{4||}$ for $\approx$ 7.5ML Ni/Cu(001) [38].

Finally we turn (Sec.2.1) to the separation of volume and surface part of the anisotropy in thin films. To separate K^{S} and K^{V} many thicknesses between 2 and 10 and 15 layers were measured. The result is shown in Fig.9 and compared to a similar experiment for Ni/W(110) films. Within the experimental error bars we see that both systems show the same surface term K_2^{S} but the volume term K_2^{V} differs by a factor of 3. In the framework of pseudomorphic growth this can be easily understood: The vacuum and interface contributions for the Ni film may be approximately the same, be it on a Cu or W substrate (mostly Néel type). However the growth and that is to say the tetragonal distortion is very much different for the two systems. On Cu(001) substrate the film growths up to 15 ML pseudomorphic with a tetragonal distortion described in Sec.2.1. On W(110) only the first 2-3 layers are distorted. For thicker films Ni growths bulk-like. In other words the K^{V} contribution is much smaller. A more detailed description goes beyond the present overview, we refer to [38].
In conclusion: the angular dependence of the intrinsic anisotropy is in theory and experiment well understood and explains nicely continuous as well as abrupt spin reorientation transitions. The temperature dependence of the anisotropy as shown experimentally in Fig.6-9 needs new theoretical input. The classical work for magnetic insulators is based on a discrete multiplet structure which is populated by Boltzmann statistics. For Fe, Co, Ni ferromagnets an itinerant theory of ferromagnetism at finite temperatures would be adequate.

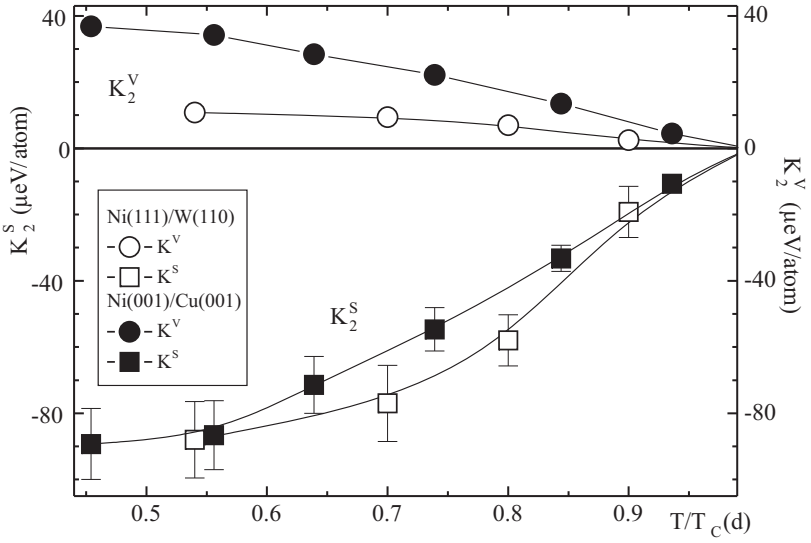

Fig. 9. Separation of the intrinsic anisotropy into surface and volume contributions for Ni(111)/W(110) and Ni(001)/Cu(001) and its temperature dependence. Note that such a diagram should be only plotted as function of the reduced temperature because by changing the thickness of the film also the Curie-temperature $T_C(d)$ changes.

3 Anisotropic magnetic moments

Several of the recent popular experimental techniques to investigate itinerant ferromagnets depend on the existence of a uniform magnetization (be it macroscopic or microscopic), e.g. spin-polarized photoemmission, magneto-optic Kerr effect, etc.. The magnetic response in these techniques vanish if the magnetization, that is to say the expectation value $\langle S_z \rangle$, vanishes. In some of the literature it is stated that the 'magnetic moment vanishes at T_C'. Similar interpretation is given if experimental findings are explained within the Stoner-Wolfarth model only. This can hardly explain the existence of magnetic moments per atom above T_C. On the other hand it is well established for more than 70 years that Fe, Co and Ni show a Curie-Weiss like behaviour above their Curie-temperatures. In the discussion of band ferromagnetism we would like to turn the focus again on the expectation value $\langle S^2 \rangle$. If for simplicity we ignore higher order effects of kT at the Fermi energy E_F, one might say that the magnetic moment per atom in ferromagnets like Fe, Co and Ni has a fixed (not integer) value which is temperature independent above and below T_C. For a detailed discussion of the distinction between $\langle S_z \rangle$ and $\langle S^2 \rangle$ see [40]. A good quantity to describe the magnetic moment/atom is the g-value or the g-tensor in solids respectively. Appropriate experimental techniques to determine this quantity are for example the susceptibility or the paramagnetic resonance. In [41] we did follow the magnetic resonance signal in thin Ni films starting in the paramagnetic phase through the

phase transition (with spin fluctuations at T_C) into the ferromagnetic phase. Furthermore it is also clear from bulk magnetism that the magnetic moment of Fe, Co, Ni is anisotropic in the bulk, e.g. the magnetic moment for a Ni single crystal along the [111]-direction is larger than along the [001]-direction (Fig.1). This anisotropy in the bulk is quite small, but finite [17].

3.1 g-tensor

The tensor character of g originates from the non-spherical charge distribution of the d-shell, that is to say of a not complete quenching of the orbital momentum. Strictly speaking $\langle L_z \rangle \neq 0$. We refer to Kittel's formula

$$\frac{g-2}{2} = \frac{\mu_L}{\mu_S} \tag{7}$$

It is known that the 'g-factor' for bulk Fe, Co, Ni is $g \geq 2$. It ranges from $g = 2.09$ for Fe to $g = 2.18$ for Co and $g = 2.21$ for Ni. In other word we have always an admixture of $4 - 10$ % of orbital magnetism. For bulk magnetism this is tabulated in textbooks [18]. We also see that within second order perturbation theory the departure from $g = 2$ comes from the same type of matrix element the anisotropy energies [28].We note that this reason for anisotropy in the magnetic moment and anisotropy energy does not depend on the use of a localized picture; it applies equally for d-bands within an itinerant picture [42].

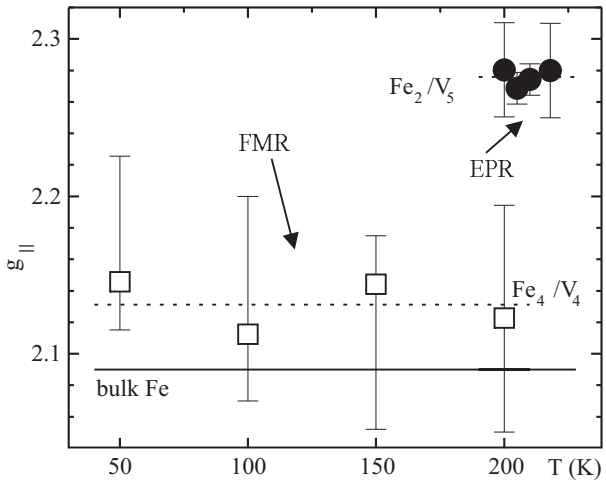

Fig. 10. g-tensor component in the film plane ($g_{||}$) of Fe_n/V_m-multilayers [43]. Note that within the error bars the g-values (i.e. the magnetic moment) are temperature independent.

In Sec.2.1 we have demonstrated that in thin film magnetism the departure of the crystallographic structural from cubic symmetry caused by pseudomorphic growth leads to lower (tetragonal) symmetries. On that basis we must conclude that also the g-value for itinerant ferromagnets departs stronger from $g = 2$ compared to bulk single crystals. As an example we show in Fig.10 $g_{||}$ (in plane) for ultrathin Fe_n/V_m-multilayers. The figure shows the bulk g-value of Fe to be $g = 2.09$. The Fe_4/V_4-multilayer has a Curie-temperature $T_C \geq 500$ K. In Fig.10 we show the determination of $g_{||}$ in the ferromagnetic phase from $50 - 200$ K to be $g = 2.13$. If one reduces the Fe-thickness down to Fe_2/V_5 the Curie-temperature decreases to $T_C \approx 200$ K. Its g-value in the paramagnetic phase was determined to be $g = 2.26$. Qualitatively this can be easily understood from the schematic drawing in Fig.7. For two layers of Fe, each of the Fe-layers faces an interface with a 'stronger symmetry breaking' and one ends with less quenching of $\langle L_z \rangle$. A detailed discussion with correlation to the change of the easy axis of magnetization etc. will be published elsewhere.

3.2 X-ray magnetic circular dichroism at 3d L-edges

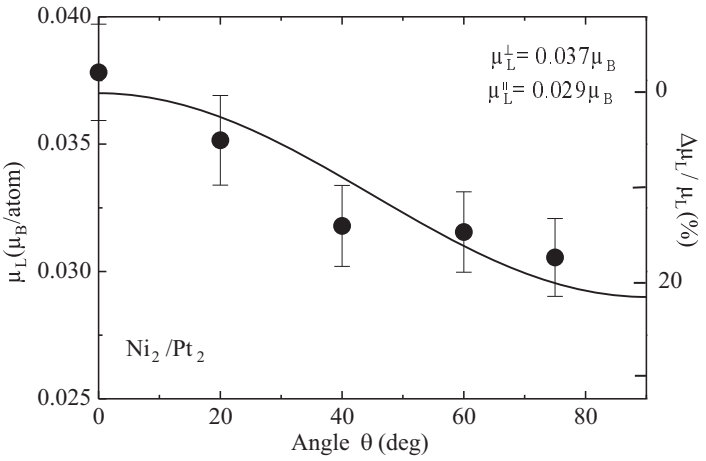

Fig. 11. Anisotropy of the orbital moment μ_L for Ni_2/Pt_2-multilayers determined from XMCD [44].Although the absolute value of μ_L is small its relative change is dramaticly large, namely 22 %.

The recent progress in XMCD [7–11] allows also to determine the orbital moment μ_L and spin moment μ_S (see also the chapter by H. A. Dürr in this book). Using the sum rules for the analysis of $L_{3,2}$ edge XMCD one may determine the orbital moment μ_L and its anisotropy $\Delta\mu_L$. As an example [44] we show the angular dependent XMCD for a Ni_2/Pt_2-multilayer structure in Fig.11. This film has its easy axis of magnetization perpendicular to the film plane, i.e. at $\theta = 0°$.

Fig.11 shows that for this direction the orbital moment is largest and reduces for the in-plane ($\theta = 90°$) direction. This is in accordance with the general rule that the magnetic moment is largest along the easy axis of magnetization (this rule has some exceptions). One might say that μ_L/atom is very small (left hand y-axis). On the other hand the relative change in % is extremely large, namely 22 %. Since the total moment per Ni-atom is very small $\approx 0.6\mu_B$, it is no surprise that the orbital moment is only a few % of μ_S. Important is the relative change of μ_L. Indeed the MAE (Sec.2) for these ultrathin Ni/Pt-multilayers is $10 - 100$ times larger compared to a bulk Ni single crystal [44].
Finally we note that a precise determination of μ_L from XMCD relies on a proper determination of the area under the dichroic signal at the L_3- and L_2-edges. The application of the sum rules [9,10] is underlying a localized picture, namely to assume a step-like change of the absorption coefficient at the $L_{3,2}$-edges. Further theoretical work will be needed for an adequate description of itinerant systems [45]. These authors separate the configuration of occupied electron states in Ni into a localized and delocalized part. First attempts to separate one-electron and multi-electron features as well as localized and delocalized parts in the analysis of XMCD for Ni has been made [46].

4 Summary

In this contribution we tried to distinguish between anisotropic magnetic moments and macroscopic anisotropy energies. In most solids with lower than cubic symmetry the magnetic moment per atom is anisotropic also in the paramagnetic phase. The moments are randomly oriented: with equal population along +/- direction and the net magnetization is zero ($\langle \mu_z \rangle = 0$). Only below the ordering temperature at which a cooperative alignment of the moments starts we measure a net magnetization $\langle \mu_z \rangle \neq 0$. To rotate this magnetization from the easy axis (lowest energy) into the hard direction costs energy. This energy increases by reducing the temperature up to its maximum value at $T = 0$. In the framework of second order perturbation theory it is said that the anisotropy energy is proportional to the anisotropy of the orbital magnetic moment $K \propto \Delta\mu_L$. That can hold only for $T = 0$.
The enormous research on ultrathin films and nanostructures opened a complete new field in experiment and theory to study the fundamental understanding of magnetism: In the research of bulk magnetism we did have only three fixed Curie-temperatures for Fe, Co and Ni ($\approx$ 1000 K, $\approx$ 1300 K, $\approx$ 600 K). In ultrathin films due to finite size effects we are now in a position to manipulate for each of the 3 ferromagnets the Curie-temperature from its bulk value down to almost zero K (for 1.6ML Ni a T_C of 36 K has been measured). Consequently, susceptibility, g-tensor, MAE and other measurements can be performed for the whole temperature range. That is to say, a reduction in film thickness offers not only a transition from 3D $\rightarrow$ 2D, it is equally interesting to manipulate the ordering temperature. New experiments and theory which clearly distinguish

between the two observables $\langle \mu^2 \rangle$ and $\langle \mu_z \rangle$ will lead to a better understanding of basic properties of magnetism.

5 Acknowledgments

We enjoyed fruitful collaboration with theory groups of B. Johansson, O. Eriksson, K. H. Bennemann, W. Nolting, P. Weinberger, H. Ebert, R. Wu as well as the experimental groups of K. Heinz, D. Arvanitis. J. Lindner is acknowledged for preparation of this manuscript and helpful comments. The work is supported by BMBF, Grant 05 SC8 KEA-3 and DFG, SFB 290.

References

1. S. Chikazumi: *Physics of Magnetism*, 2nd edn. (John Wiley, New York 1964) and S. Chikazumi, C. D. Graham, JR: *Physics of Ferromagnetism*, 2nd edn. (Oxford University Press, 1997)
2. E. Kneller: *Ferromagnetismus*, (Springer, Berlin, Göttingen, Heidelberg 1962)
3. B. Coqblin: *The electronic Structure of Rare-Earth Metals and Alloys: The magnetic Heavy Rare-Earths*, (Academic Press London, New York, San Francisco 1977)
4. J. Kübler: *Theory if Itinerant Electron Magnetism*, (Clarendon Press, Oxford 2000)
5. B. Heinrich and J. A. C. Bland: *Ultrathin Magnetic Structures*, (Springer, Berlin 1994)
6. A. J. Freeman, S. D. Bader: *Magnetism beyond 2000*, (Elsevier, Amsterdam, Lausanne, New York, Oxford, Shannon, Singapore, Tokyo 1999)
7. B. T. Thole et al.: Phys. Rev. Lett. **55**, 268 (1985); G. van der Laan et al.: Phys. Rev. B **34**, 6592 (1986)
8. G. Schütz, W. Wagner, W. Wilhelm, P. Kienle, R. Zeller, R. Frahm, G. Materlik: Phys. Rev. Lett. **58**, 737 (1987)
9. B.T. Thole, P. Carra, F. Sette, G. van der Laan: Phys. Rev. Lett. **68**, 1943 (1992); P. Carra, B. T. Thole, M. Altarelli, X. Wang: Phys. Rev. Lett. **70**, 694 (1993)
10. M. Altarelli: Phys. Rev. B **47**, 597 (1993)
11. A. Ankudinov, J. J. Rehr: Phys. Rev. B **51**, 1282 (1995)
12. R. Q. Wu, L. J. Chen, A. Shick, A. J. Freeman: J. Magn. Mater. Mater. **177-181**, 1216 (1998)
13. J. Trygg, B. Johansson, O. Eriksson, J. M. Wills: Phys. Rev. Lett. **75**, 2871 (1995); O. Eriksson, B. Johansson, R. C. Albers, A. M. Boring, M. S. S. Brooks: Phys. Rev. B **42**, 2707 (1990)
14. G. Y. Guo, H. Ebert, W. M. Temmerman: J. Phys.: Condensed Matter **3**, 8205 (1991)
15. G. T. Rado, H. Suhl: *Magnetism*, vol. 1-5, (Academic Press New York, London 1973)
16. Callen H B and Callen E R: J. Phys. Chem. Solids **27**, 1271 (1966)
17. Landolt-Börnstein: *Vol.III/19a, ed. by H.P.J. Wijn*, (Springer-Verlag, Heidelberg 1986)
18. A. Abragam, B. Bleaney: *Electron Paramagnetic Resonance of Transition Ions*, (Clarendon Press, Oxford 1970)

19. A. Hubert, R. Schäfer: *Magnetic Domains* (Springer, Heidelberg 1998)
20. K. Baberschke: Surf. Sci. Lett. **6**, 735 (1999)
21. O. Hjortstam, K. Baberschke, J. M. Wills, B. Johansson, O. Eriksson: Phys. Rev. B **55**, 15026 (1997)
22. W. Platow, U. Bovensiepen, P. Poulopoulos, M. Farle, K. Baberschke, L. Hammer, S. Walter, S. Müller, K. Heinz: Phys. Rev. B **59**, 12641 (1999)
23. B. Schulz and K. Baberschke: Phys. Rev. B **50**, 13467 (1994)
24. X. Wang, R. Wu, D.-S. Wang, A. J. Freeman: Phys. Rev. B **54**, 61 (1996)
25. L. Néel: J. Physique Radium **15**, 376 (1954)
26. U. Gradmann: J. Magn. Magn. Mater. **100**, 481 (1991); U. Gradmann: J. Magn. Magn. Mater. **54/57**, 733 (1986)
27. M. Farle, W. Platow, E. Kosubek, K. Baberschke: Surf. Sci. **439**, 146 (1999)
28. K. Baberschke: Appl. Phys. A **62**, 417 (1996)
29. C. Uiberacker, J. Zabloudil, P. Weinberger, L. Szunyogh, C. Sommers: Phys. Rev. Lett. **82**, 1289 (1999)
30. K. Baberschke, M. Farle: J. Appl. Phys. **81**, 5038 (1997)
31. A. Aspelmeier, F. Gerhardter, K. Baberschke: J. Magn. Magn. Mater. **132**, 22 (1994)
32. E. D. Tober, R. X. Ynzunsa, C. Westphal, C. S. Fadley: Phys. Rev. B **53**, 5444 (1996)
33. M. Farle, K. Baberschke: Phys. Rev. Lett. **58**, 511 (1987) and M. Farle, A. Berghaus, K. Baberschke: Phys. Rev. B **39**, 4838 (1989)
34. B. Heinrich, K. B. Urquhart, A. S. Arrott, J. F. Cochran, K. Myrtle, S. T. Purcell: Phys. Rev Lett. **59**, 1756 (1987)
35. A. Berghaus, M. Farle, Yi Li, K. Baberschke: Springer Proc. in Physics **50**, 61 (1989)
36. P. Poulopoulos, K. Baberschke: J. Phys.: Condensed Matter **11**, 9495 (1999)
37. M. Farle, B. Mirwald-Schulz, A. Anisimov, W. Platow, K. Baberschke: Phys. Rev. B **55**, 3708 (1997) and M. Farle, W. Platow, A. Anisimov, B. Schulz, K. Baberschke: J. Magn. Magn. Mater. **165**, 74 (1997)
38. M. Farle: Rep. Prog. Phys. **61**, 755 (1998)
39. A. N. Anisimov, W. Platow, P. Poulopoulos, W Wisny, M Farle, K. Baberschke, P. Isberg, B Hjörvarsson, R. Wäppling: J. Phys.: Condens. Matter **9**, 10581 (1997)
40. D. K. Wohlleben, B. R. Coles in vol. 5 of ref. 15 and references therein
41. Y. Li, K. Baberschke: Phys. Rev. Lett. **68**, 1208 (1992)
42. P. Bruno: Phys. Rev. B **39**, 865 (1989)
43. A. N. Anisimov, M. Farle, P. Poulopoulos, W. Platow, K. Baberschke, P. Isberg, R. Wäppling, A. M. N. Niklasson, O. Eriksson : Phys. Rev. Lett. **82**, 2390 (1999)
44. F. Wilhelm, P. Poulopoulos, P. Srivastava, H. Wende, M. Farle, K. Baberschke, M. Angelakeris, N. K. Flevaris, W. Grange, J.-P. Kappler, G. Ghiringhelli, N. B. Brookes: Phys Rev. B **61**, 8647 (2000)
45. A. L. Ankudinov, A. I. Nesvizhskii, J. J. Rehr: J. Synchroton Rad. **8**, XXX (2001)
46. A. I. Nesvizhskii, A. L. Ankudinov, J. J. Rehr, K. Baberschke: Phys Rev. B **62**, 15295 (2000)